UNIVERSITY OF THE
WEST *of* SCOTLAND
UWS

UWS Academic Portal

Numerical modelling and CFD simulation of a polymer electrolyte membrane (PEM) fuel cell flow channel using an open pore cellular foam material

Awotwe, Tabbi; Khatib, F.N.; Ijaodola, O.S.; Ogungbemi, E.; El-Hassan, Zaki; Durrant, A.; Thompson, J.; Olabi, A.G.

Document Version
Peer reviewed version

[Link to publication on the UWS Academic Portal](#)

Science of the total environment
ARTICLE

Numerical Modelling and CFD Simulation of a Polymer Electrolyte Membrane (PEM) Fuel Cell Flow Channel Using an Open Pore Cellular Foam Material

Tabbi Wilberforce[1] , F. N. Khatib[*1], O. S. Ijaodola[1], E. Ogungbemi[1], Zaki El - Hassan[1], A. Durrant[1], J. Thompson[1], A. G. Olabi[2,3]

1. Institute of Engineering and Energy Technologies, University of the West of Scotland, PA1 2BE, UK

2. Dept. of Sustainable and Renewable Energy Engineering, University of Sharjah, P.O. Box 27272, Sharjah, UAE

3. Mechanical Engineering and Design, Aston University, School of Engineering and Applied Science, Aston Triangle, Birmingham, B4 7ET, UK

ABSTRACT

Fuel cell performances varies with different structural configurations and materials. However, the two main areas that determine this performance metric are the membrane electrode assembly (MEA) and the bipolar plates. The MEA provides the platform for the electrochemical reaction to occur and the bipolar plate serves as a medium between the reactants (hydrogen and air) and the catalyst layer. The bipolar plate is the first point of contact for the reactants inside the fuel cell, so a badly designed item with a high pressure drop will have a negative impact on fuel cell performance. Numerical modelling and simulation tools like ANSYS have a huge impact on engineering industry as they help designs to be validated and analysed before any physical construction.

This investigation considers five suitable flow plate designs for PEM fuel cell, each completely different from the readily available, traditional serpentine designs on the market. The work explored the possibility of replacing these flow channels with an aluminium cellular foam with different inlet and outlet orientations. The designs were further optimised and modelled in ANSYS.

1

26   The results obtained were compared with other designs in the literature. Compared to the

27   serpentine flow design, the open pore cellular foam material showed a very small pressure drop in

28   the range of 30-40 Pa. This indicates a possibility of replacing the traditional flow plate designs

29   with the proposed ones.

30   **Key words**: Computational Fluid Dynamics (CFD), Optimization, Fuel cell, Serpentine, Design

31   of Experiment (DOE)

32   **INTRODUCTION**

33   Fuel cells are electrochemical devices that transform the chemical energy of reactants into

34   electrical energy with a very high efficiency. Fuel cells produce waste heat and generate water as

35   a reaction product. The fuel (hydrogen) is supplied to the negative electrode (anode) while the

36   oxygen from air being the oxidant is supplied to the positive electrode (cathode) as seen in Proton

37   Exchange Membrane fuel cells, among others. The chemical reaction at the anode produces

38   electrons for an electric current. All fuel cells have very high efficiencies which are often

39   independent on the size of the system. Their design is also scalable and they produce zero or

40   almost zero greenhouse gas emissions. As they have no moving parts, their operation is highly

41   reliable as a result of their being vibration-free and less susceptible to wear and tear [1]. Fig. 1

42   shows a 3D view of a five stack fuel cell.

43   Though the advantages of fuel cells are enormous, their disadvantages cannot be overlooked. Cost

44   remains a major challenge to the fuel cell industry, which has impaired their commercial success

45   for general use. Storage of pure hydrogen is also a major issue. In situations where fuel that is not

46   pure is used, additional fuel reformation technology has to be taken into account. Fuel cell

47   performance also decreases when impure hydrogen gas is used. Traditional power generation

largely depends on fossil fuels which are now being discouraged around the world because of their

high impact on the environment. Fuel cells are used for a number of portable applications, in the

transportation sector and even the stationary sector. Most scientists believe that portable devices

like mobile telephones and laptop computers will soon demand high power to keep them running

for longer. As fuel cells are scalable with very simple recharging capabilities compared to batteries,

they are a suitable option for portable devices in the near future. The limitations of fossil fuels and

the high demand for them by the transport industry contribute to fluctuations in prices,

necessitating an alternative energy source. In its defence, the transport industry has undergone

significant recent improvement as there is a growing number of hydrogen fuel cell cars on today's

roads, with researchers still conducting investigations to improve the current automobile

technology to develop a product that is cheaper and more reliable. The unreliability of the power

supply in some parts of the world affects most companies negatively [2]; an improvement in

current fuel cell technology will do much to alleviate this. In order to generate more electricity and

heat for living space, the stationary fuel cell is usually preferred. There are currently eight types of

fuel cells available: Alkaline Fuel cells (AFCs), Phosphorous Acid Fuel cell (PAFCs), Solid Oxide

Fuel Cells (SOFCs), Molten Carbonate Fuel cells (MCFCs), Zinc-air fuel cells (ZAFCs), Protonic

Ceramic Fuel cells (PCFCs), Biological fuel cells (BFCs) and Proton Exchange Membrane fuel

cell (PEMFCs)[2,3]. The PEMFC, also called the polymer electrolyte cell, generates a high power

density at low weight, cost, and volume. PEMFCs are normally made up of an anode, cathode and

an electrolyte membrane as shown in Fig. 2.

Oxidation of hydrogen occurs at the anode while reduction of oxygen occurs at the cathode. The

electrons are transported from one to the other through an electric circuit, hence the fuel cell is

used as a DC source. The fuel cell has a carbon paper, mainly for covering the electrolyte on both

71 anode and cathode sides of the fuel cell. The porosity of this backing layer is normally in the range

72 0.3 to 0.8. It plays a vital role in the transfer of the reactants as well as the reaction product to the

73 flow plate of the reactive sites [3]. While the electrons produced at the anode are drawn away into

74 the electric circuit, the ions that also result from the electrochemical reaction travel through the

75 electrolyte to cathode. At the cathode, an electrochemical reduction occurs due to the electrons

76 returning from the external load. One actively used electrolyte material, Fluorinated Teflon by

77 Dupont, is mostly used in PEM fuel cells and referred to as a "Nafion membrane", as shown in

78 Fig. 3.

79 Nafion membranes provide a high chemical reaction and thermal stability. The electrodes are thin

80 films that are well attached to the membrane. Electrodes with a low platinum loading perform well

81 compared to those with a high platinum loading. Adding the polymer in a soluble state into the

82 pores of the support structure (carbon) is one of the approaches taken to improve the usage of the

83 platinum. The interface between the electrocatalyst and solid polymer electrolyte is increased by

84 adapting this approach. Water management in the fuel cell is very crucial, as less or more water

85 could damage the fuel cell. Therefore fuel cell design must carefully consider flooding and its

86 prevention. The electrochemical reaction produces water which is expected to leave the cell after

87 the electrochemical process but poor cell design means it is produced faster than its rate of escape..

88 This flooding prevents the MEA from functioning at its full potential hence nearly one-third of the

89 MEA surface is utilised. [4-6]. The bipolar plates and the membrane electrode assembly are the

90 two most important parts of the fuel cell. The transport of the reactants to the reactive site occurs

91 through the bipolar plate. The membrane electrode assembly, having the platinum catalyst layer

92 on its surface, functions as the platform where the electrochemical reaction occurs. Supplying

93 reactant at high concentrations to the catalyst layer with less obstruction will therefore significantly

94 improve fuel cell performance. The design of the bipolar plate is also important as it determines

95 the water management through the cell and creates a platform where the generated current can be

96 collected [7]. The membrane electrode assembly is often located between two flow plates. It is

97 composed of a proton exchange membrane and a gas diffusion layer which is porous in nature but

98 conductive electrically. Bipolar plates in the fuel cell are normally made of graphite with a metallic

99 housing but this design is gradually falling out of practice. Most newly developed PEM fuel cells

100 are made of a polymer called acetyl to reduce the weight of the fuel cell, which in effect reduces

101 its overall cost [8-10]. Fig. 4 shows some new types of fuel cell on the market that use acetyl.

102 Though graphite has some good electrical properties, it has some major setbacks that have

103 prompted the paradigm shift by researchers around the world from relying on it as the sole material

104 for the bipolar plate. The tensile strength of graphite is very low and it is also very brittle. It is also

105 very expensive to machine. With the bipolar plate accounting for almost 70% of the weight of the

106 entire cell according to Lawlor et 2009, Dong *et al.*, 2007 [11, 12], it is recommended that the

107 material for the bipolar plate be made lighter as nearly 40% of the cost of a fuel cell depends on

108 the bipolar plate.

109 Metals have recently become more popular as the material of choice for bipolar plates as their

110 advantages include low cost, ease of processing, high mechanical strength, high electrical

111 conductivity and high thermal conductivity. The normal practice is for the flow channels to be

112 machined on the bipolar plate. This is done to achieve uniform distribution of the reactants and

113 thus helps make better use of the MEA. The flow channel can be straight, parallel and even

114 serpentine [11 – 15]. Other investigations concluded that the performance of any fuel cell is highly

115 dependent on the bipolar design [13 – 20]. This is simply because a poorly designed bipolar plate,

116 as mentioned earlier, often leads to problems with water removal and obstructs reactant transport.

5

117   Another researcher undertook a detailed study of the various types of flow plates in a fuel cell and

118   also recommended that, for effective fuel distribution, the bipolar plate must be carefully designed

119   [21]. It therefore confirms that an improperly designed bipolar plate will lead to uneven

120   distribution of the electrochemical reactant in the fuel cell, which reduces the utilisation of the

121   catalyst layer [22]. Open pore cellular foam (OPCF) material has recently been used by a number

122   of researchers around the world as an alternative to the traditional flow field design. This is simply

123   because the gas distribution through the OPCF material is fairly even, overcoming the poor

124   distribution in other set-ups. Again, the pressure drop between the inlet and outlet through the open

125   pore cellular foam material (OPCFM) is subject to the size of the pores of the foam [23 – 25]. Fig.

126   5 shows an OPCFM with a porosity of 90% obtained from Goodfellow, UK.

127   Carbon foam has been utilised as the gas flow field was first proposed by Marice *et al.* [26]. Other

128   researchers, like Tsai *et al/* [27], also confirmed that flow plate material made of metal foam

129   contributed significantly to the efficiency of the fuel cell. They critically explored the effect that

130   flow plate design had on the efficiency of PEM fuel cells. Their investigation brought to light that

131   flow plate designs play an active role when building a fuel cell using foam material or even the

132   traditional fuel cell designs. Kumar and Reddy [28, 29] used foam material in place of channels of

133   conventional flow plates. This modification is not considered appropriate as the full benefit of the

134   OPCFM was not explored. With all these advantages of using the OPCF, researchers are still facing

135   challenges in relation to the housing unit where the foam will be placed. The present work is an

136   extension to earlier work [2] where in this investigation a newer approach to the designs have been

137   carried to optimise the use of Open Pore cellular foam materials. This paper seeks to investigate a

138   new housing unit for the OPCF material, where the results are analysed on the pressure, flow

139   regimes and velocity profiles.

140   There has been a big increase in the precision of engineering designs as scientists are better able

141   to predict the success or failure of their designs by simulation, thus saving time and money

142   Computational fluid dynamics (CFD) simulation software is one such example, as it can predict

143   and analyse the various flow regimes in a fuel cell design and, in some cases, compute the stresses

144   as well. Research into the development and optimisation of flow plates has been studied using

145   CFD simulations [30-37]. Apart from many uses, CFD is also capable of providing information

146   about the distribution of pressure through the flow channel, the pattern of the pressure and the drop

147   in pressure. The velocity at which material enters and leaves the PEM fuel cell can all be predicted

148   using the CFD tool. With this information obtained from the CFD simulation, designers can easily

149   create or modify their designs without wasting energy in the workshop on ideas that are not feasible

150   or practical. One of the important factors considered in a fuel cell is the even distribution of the

151   oxidant (air/oxygen) and fuel (hydrogen) on the Gas diffusion layer. The pressure of these reactants

152   must be distributed evenly over the Gas Diffusion Layer. This is very important as it determines

153   the amount of catalyst being utilised during the electrochemical process. These are the parameters

154   that define fuel cell performance. The flow channels on the bipolar plates serve as the medium to

155   supply and uniformly distribute the oxidant and fuel to the catalyst layer. CFD analysis to help

156   predict the flow distribution across the channels and check the pressure and velocity through the

157   bipolar plate channels was performed by Kumar and Reddy, 2003, [33], Lozano *et al.*, 2008 [36]

158   and Barreras *et al.* 2011 [37]. This research work intends to explore other suitable flow plate

159   designs using OPCF material. The designs were optimised and varied across selected velocities in

160   literature (1, 3, 6, 9, 12 m/s). Different types of manifold designs were considered and their flow

161   regimes were checked through CFD simulation analysis.

162   **NUMERICAL MODELLING, OPTIMISATION AND SIMULATION**

7

163 As explained earlier, pressure distribution on the gas diffusion layer and the membrane electrode

164 assembly are important parameters when designing a fuel cell. Other factors, like temperature

165 distribution and even the speed at which the reactive gases travel to the reactive site are all very

166 important as they influence the output or efficiency of the cell. The outcome of the simulation can

167 also clearly show areas in the design where there could be the possibility of dead zones. Dead

168 zones are areas around the fluid domain where the gas is static. It could also be described as the

169 area around the fluid domain that may not be in contact with the reactive gas. This leads to

170 accumulation and retention of water in the cell. A vital function of the gas is to be able to carry

171 any water along the channels as it flows towards the outlet of the channel. Accumulation of water

172 prevents some areas on the MEA from being utilised, hence reduces fuel cell performance.

173 Excessive water in the fuel cell could cause flooding of the cell which will also create serious

174 problems in the functionality of the PEM fuel cell. This clearly stipulates that the design of bipolar

175 plate even affect the water management in the cell.

176 **FUEL CELL DESIGN**

177 ANSYS software was used to determine the flow regimes for the bipolar plate of a fuel cell with

178 an active reaction area of 25 cm^2. A number of designs were suggested for the bipolar plate to aid

179 in the channelling of hydrogen to the reactive sites of the MEA. Manifolds were created in order

180 to channel the hydrogen towards the foam material. CFX in ANSYS was used as the CFD

181 technique to analyse housing designs for both the anode and cathode regions of the fuel cell. The

182 electrochemical reaction in a PEM Fuel cell operates under moderate conditions when compared

183 to the other types of fuel cell. The rate at which the various reactive gases travel through the bipolar

184 flow plate design may be low but the fuel cell will still produce some current. Theoretically, it is

185 possible to calculate the pressure drop in the fluid domain but the type of flow must first be

8

186 determined. The flow could be laminar or turbulent. This is determined through the calculation of

187 the Reynolds number. For the purpose of this investigation, the flow was considered laminar since

188 it has been well established that the reactants inside the fuel cell are in laminar flow, with a

189 Reynolds number Re < 2300. The flow was also kept as a single phase. The laminar flow design

190 was also utilized by Ramos – Alvarado *et al.* [38]. Various designs were then simulated with

191 specific boundary conditions clearly depicted in Table 1. The final model contained 290,000 –

192 316,853 elements. Fig. 6 shows the anode housing designs with their respective CFD mesh using

193 ANSYS CFX.

194 Table 1: Boundary conditions used in running the simulations.

Parameter	Response
Design Modeller	CFX
Mesh	Mixed Tet and Quad
Sizing	Proximity and Curvature
Smoothing	Fine
Transition	Fast
Elements	316,853
Solver	CFX
Model flow	Laminar
Fluid	Hydrogen
Solid walls	Aluminum
Porosity	0.93

9

Inlet Velocity	1m/s
Temperature	320
Monitors	Mass flow Continuity
Interfacial area density	0.50
Heat transfer coefficient	0.01
iteration	100
Solver type	Pressure based – Double precision

199   From Table 1, the meshing was kept as Mixed Tet and Quad and a fine mesh was generated. The

200   number of elements was also 316,853. The fluid domain for the gas was kept as being porous and

201   the porosity of the aluminium foam used was 0.93. The speed of the gas entering the fuel cell was

202   also maintained at 1 m/s and the flow kept as laminar. The number of iterations was also kept at

203   100 for convergence to occur during the simulation. The sizing of the mesh was also maintained

204   at proximity and curvature but during the simulation for design 5, which is the serpentine flow

205   channel, the fluid domain was maintained in settings since the channel was not porous.

206   NUMERICAL MODEL

207   Extensive research in the design of metal foams have been undertaken, where key characteristics

208   that determine the performance of the foam has been established both experimentally and

209   theoretically [38-45]. One of the performances measured is the pressure drop in the foam material

210   and different mathematical models have been developed. Flow in a porous media can be

211   determined by the well known Darcy's Law [45]:

212212

$$\Delta P \qquad v$$

10

213213 $$\frac{}{L} = \left(\frac{}{\gamma}\right) V \tag{1}$$

11

214

215   Where, ΔP is the pressure drop over length L (m), v is the fluid viscosity (m²/s), V is the fluid

216   velocity (m/s) and γ (m²) describes the permeability of a porous media. However, Darcy's law can

217   be used only for low Reynolds numbers (Re < 0.1). In instances where there are high flow

218   velocities (>0.1 m/s), the drag induced by the ligaments of the foam material becomes important.

219   There is also a major influence of both turbulence and inertia and the pressure drop therefore

220   displays a parabolic trend with the increasing velocity [46]. Therefore to consider this, a modified

221   form of D'Arcy model, that describes the pressure drop in the porous medium at these velocities

222   also known as the Hazen Dupuit-Darcy model is used,

223

224   $$\frac{\Delta P}{L} = \frac{v}{\gamma}V + \rho C V^2 \tag{2}$$

225

226   Where, ρ is the density of the gas in the medium (kg/m³), and, $C = f/\sqrt{\gamma}$ is the coefficient related

227   to the structure of the permeable medium, with f being the coefficient of inertia. The permeability

228   γ (m²) of porous media is related to the porosity and the mean pore radius, is given by [38],

229

230   $$\gamma = \frac{\zeta^3}{180(1-\zeta)^2}d_p{}^2 \tag{3}$$

231

232   Where, ζ is the porosity of the foam material and d_p is the pore diameter. For the traditional hollow

233   (serpentine) channels, since the flow is laminar in a functional PEMFC, one can define

234   permeability, γ for the channel through the well-known Hagen–Poiseuille equation [38],

12

235 $$\gamma = H\,\frac{d_h{}^2}{32} \tag{4}$$

236 Where, $H = 2.59$ (m) is the shape factor which is typical for laminar flows [38], d_h is the hydraulic

237 diameter of the channel (m).

238 Another mathematical model, by Ergun *et al.* determines the pressure drop in the foam material

239 with spherical particles of diameter d_p. The Ergun equation is commonly utilized where the flow

240 is through a dense bed, however, to draw a comparison between different mathematical models,

241 this equation was also used.

242

243 $$\frac{\Delta}{L} = AV + B\rho V^2 \tag{5}$$

244

245 Where,

246 $$A = \frac{150(1 - \zeta)}{\zeta^3 d_p{}^2} \tag{6}$$

247 $$B = \frac{1.75(1 - \zeta)}{\zeta^3 d_p} \tag{7}$$

248 Research in the design and fabrication of metal foams with different manufacturing techniques has

249 also been undertaken [47], where Ashby *et al.* mathematically define the pressure drop in the metal

250 foams as,

251 $$\frac{\Delta P}{L} = \varepsilon \left(\frac{1}{d_p}\right) \left[\frac{v^m \rho}{(1 - \alpha)^{2-m}}\right] V^{2-m} d_L{}^{-m} \tag{8}$$

13

252252

253   Where, α is the absorption coefficient, d_L is the foam ligament diameter, ε and m are determined

254   experimentally [47]. This equation is in the context of drop the in pressure with respect to transfer

255   of heat, but for the purposes of correlating models, this equation was also used. The effect of the

256   drag and friction due to flow in the foam material was explicitly described by Fourie and Du Plessis

257   [48], where they make use of the tortuosity of the ligament structure, and thus determining the

258   pressure drop as,

259259

$$\frac{\Delta P}{L} = (3 - \tau)(\tau - 1)\left(\frac{\rho\tau^2 V^2}{\zeta^3 d}\right)\left(\frac{3C_{dv}}{2} + \frac{C_{df}}{4}\right)\zeta \tag{9}$$

261   Where,

$$C_{dv} = \frac{24v\zeta}{\rho(3 - \tau)d_p V} \tag{10}$$

$$C_{df} = 1 + 10\left(\frac{\rho V^2 d_p(\tau - 1)}{2v\zeta}\right)^{-0.667} \tag{11}$$

264264

265   Where, τ is the tortuosity, C_{dv} and C_{df} are drag and frictional coefficient.

266   Since the pressure drop in the channel is directly related to the pressure gradient and the channel

267   permeability, the pumping power consumption can be approximated by the product of the pressure

268   drop along the channel and channel flow rate [38]. Wang, 2005 establishes a pumping power

269   parameter as a ratio of the pumping power for the cathode flow (the major part) of the electric

270   power produced by a fuel cell. Unlike an equation that describes the fuel cell polarisation curve, a

271   linear approximation is assumed to be a very good fit for practical operating conditions [38]. Here

272   a modified form of the equation has been established to define a linearisation of a polarisation

15

273   curve,

274     $V_{cel} = V_o - V_n$ (12)

275   Where, V_o is the intercept of the polarisation curve, as the actual open circuit voltage is always

276   higher, in the analysis, it has been maintained at 0.9 V. V_n is defined as the linear voltage drop as

277   in equation (13).

278278 $$V_n = \frac{A_m \, v \rho L I}{16 \beta_{pump} A_c} \left(\frac{\xi_c}{F C_{O_2}} \right)^2 \frac{1}{\gamma}$$ (13)

279   Where, A_m and A_c is the area of membrane and cathode respectively (m^2), v is the kinematic

280   viscosity (m^3/s), ρ is the density (kg/m^3), L is the length (m), I is the current density (A/m^2), ξ_c is

281   the stoichiometric flow ratio, F is the Faraday constant (A/mol), C_{O_2} is the concentration of oxygen

282   (mol/m^3), β_{pump} is the pumping power ratio [38].

283   **RESULTS AND DISCUSSION**

284   One of the simplest means of analysing and optimising flow field configuration is through

285   observation of the distribution of pressure and velocity in the fluid domain. As stated earlier, the

286   selected design must be able to uniformly distribute pressure over the gas diffusion layer at a

287   constant rate. The drop in pressure between the inlet and outlet of the flow channel must be less as

288   well in order for the gas to reach the reactive site early for electrochemical reaction to occur.

289   **DESIGN 1 OF FLOW CHANNEL (D1)**

290   The first observation is the collision of the fluid with the foam as it flows from the inlet. This

291   causes the speed at which the gas is travelling to increase but the obstruction causes a change in

292   direction around the manifold. Convective flow is created along the porous domain. The D1 profile

293   for the distribution of pressure and velocity is shown in Fig. 7. The purpose of this design was to

17

294 uniformly distribute the reactant gases over the open pore cellular foam material (OPCFM). The

295 inlet of the design was created to have an obstruction that was oval in shape. This was done so that

296 the gas builds up momentum as it flows around the oval impediment. The downstream part of the

297 flow plate had same features as the upstream. Convective flows are observed as the gas leaves the

298 impediment into the porous fluid domain. From the pressure profile in Fig. 7(a), the pressure of

299 the gas entering the fluid domain is at 3.2 Pa. It reduces as the gas exit the fluid domain at 1.0 Pa,

300 indicating an overall pressure drop of 2.1 Pa. The mass transport which is linked to the efficiency

301 of the fuel cell will also be seriously affected. A uniform pressure and velocity distribution are

302 observed, as shown in Fig. 7(a) and 7(b). The greater portion of the gas will flow through the foam,

303 meaning that the GDL, which will be in contact to the MEA, will have most of its surface in contact

304 with the gas. Hence the release of electrons through the electrochemical reaction will be very high

305 thereby increasing the amount of energy produced. Water found in the pores or channels will be

306 carried to the outlet easily since large areas of the design will have gas flowing through them. This

307 design will, therefore, be suitable for water management in the fuel cell and also the fewer dead

308 zones show the lesser possibility of water accumulation which affects the fuel cell negatively [40].

309309

310 DESIGN 2 OF FLOW CHANNEL (D2)

311 The D2 design can be seen in Fig. 8. It consists of an obstruction which is perpendicular to the

312 main inlet but the dimensions for each of the five(5) rectangular impediments are irregular. The

313 design is similar to D1, with the downstream section of the fluid domain same as the upstream.

314 The orientation of the inlet and outlet are diagonal to each other. The pressure distribution

315 according to the pressure profile in Fig. 8(a) shows that D2 has the pressure of the fluid being high

316 at the inlet but reduced at the outlet where the gas exits the fuel cell. From the profile, the mid

18

317 region of the design will have the pressure uniformly distributed. In comparison with D1, the inlet

318 pressure for the D2 is lower. There is, therefore, the pressure drop between the inlet region and the

319 outlet of the cell. The efficiency of the fuel cell will be greatly affected due to the effect on mass

320 transport. Greater portions of the MEA will be utilised as the gas will travel through larger portions

321 of D2 compared to that of D1. The outlet velocity for D2 shown in Fig. 8(b) is higher than that of

322 D1, hence any water in the fluid domain or channel will leave the D2 faster than it will D1. There

323 are some regions in the fluid domain of D2 that are low, which , creates dead zones and hence

324 more water accumulated in the fuel cell. It remains one of the major setbacks for this design. The

325 inlet and outlet orientation are also diagonal to each other.

326 DESIGN 3 OF FLOW CHANNEL (D3)

327 The D3 design, as shown in Fig. 9, has the orientation of the inlet and outlet being diagonal. The

328 design comes with impediments at the inlet and outlet region of the cell. These obstructions are

329 designed to be both diagonal and perpendicular to the inlet and outlet. It allows the gas to flow to

330 the other parts of the fluid domain but from the pressure profile shown in Fig. 9(a), there is pressure

331 drop from the inlet to the outlet. This drop in pressure is fairly low when compared to those of D1

332 and D2. From Fig. 9(b), a uniform velocity distribution is observed through the bipolar plate. The

333 general design of D3 will have a negative impact on the efficiency of the PEM fuel cell. This

334 occurs because of the orientation of the inlet and outlet of the fuel cell. The impediment for this

335 design does not allow the fluid to flow through the entire surface of the fluid domain hence not all

336 the surface of the MEA will be utilised. Dead zones will however be created since the gas is unable

337 to flow through every portion of the fluid domain. It indicates that only one-third of the MEA

338 surface may be utilised hence fuel cell performance will be low.

339 DESIGN 4 OF FLOW CHANNEL (D4)

19

340   The D4 design as shown in Fig.10, has the inlet and outlet of the design being symmetrically

341   aligned to the mid portion of the design. From the design shown in Fig. 10(a), the gas travels

342   through each symmetrical section of the fluid domain due to the double impediment at the inlet

343   region on both the left and right side of the design. The obstruction is actually found at the edges

344   of the fluid domain. The gas travels freely from the inlet to the outlet with no impediment at the

345   middle section of the fluid domain. The pressure drop from the inlet region to the outlet region of

346   D4 is low, hence it will have a positive effect on the mass transport of the fluid flowing through

347   the domain. The efficiency will therefore be fairly better compared to the designs discussed earlier.

348   From the velocity profile in Fig. 10(b), there is a lower velocity at the inlet when compared with

349   other designs. There is also less or minimal restriction as the gas flow directly from the inlet to the

350   outlet. This is noticed around the mid-section of the fluid domain. It is also observed that the entire

351   MEA surface would not be utilised. The blue regions in the D4 are also high hence there would be

352   more water accumulation of water which will affect the fuel cell performance.

353   DESIGN 5 OF FLOW CHANNEL (D5) (SERPENTINE FLOW PLATE)

354   The D5 design, as shown in Fig. 11, allows gas to travel through a greater portion of the MEA

355   hence it is the popularly preferred flow plate design for most PEM fuel cells. The results from the

356   simulation performed as shown in Fig. 11 exhibited high pressure at the inlet for the first bipolar

357   plate flow channel. As the gas flows through the rest of the channels, it drops gradually in terms

358   of pressure, which means that there would be high-pressure drop on the MEA. The implication is

359   that the mass transport will be affected and effectively lead to a reduction in fuel cell performance.

360   The velocity profile is shown in Fig. 11(b). It clearly shows that the velocity at which the gas

361   travels will be distributed evenly across the whole flow plate design. Due to the nature of the

362   serpentine design, it is able to carry all water in the channel to the outlet hence very effective in

20

363   mitigating issues relating to flooding . The velocities of some of the layers at the boundaries are

364   observed to be low particularly around the edges. Annular flows are therefore created as the water

365   is moved to the channel walls. The area marked blue shows the part of the fluid domain where

366   there dead zones could accumulate. Dead zones as defined earlier are sections on the fluid domain

367   where the gas may not travel through due to the design of the flow plate.

368   VALIDATION OF RESULTS

369   Some specific velocities used in literature (1, 3, 6, 9, 12 m/s) [9] were integrated into ANSYS. The

370   simulation was carried out to give a detailed idea of various situations that may occur in the fluid

371   domain as the gas moved from the inlet to the outlet. It therefore showed the drop in pressure for

372   each design as the gas travelled through the fluid domain at different velocities. It was noticed that

373   the drop in pressure for the D5 (Serpentine design) was high compared to the other design that was

374   aimed at using OPCF material. Fig. 12 shows the effect on pressure drop as the specific fluid inlet

375   velocities is varied in the range 1 m/s – 12 m/s for designs D1 – D5. It can be observed in Fig. 12,

376   that D4 shows a very low-pressure drop, with a maximum of 20 Pa at a flow velocity of 12 m/s.

377   The inset in Fig. 12 shows the pressure drop for a serpentine flow channel at a range of flow

378   velocity 1 – 12 m/s, where the pressure drop is very high even at low flow velocities. In contrast

379   to the traditional flow channels, the use of OPCF material shows better performance

380   characteristics. Table 2 shows the boundary conditions that were used to run the optimisation of

381   the flow plate.

382382

383383

21

384   Table 2 – Boundary conditions used in the simulation of the flow plates using Velocity

Meshing Properties		Boundary Conditions		Solution Parameters	
Mesher	ANSYS meshing	Model	OPCF	Solver	CFX
Mesh	Proximity and Curvature	Viscous model	Laminar	Solver type	Pressure based
Relevance	Fine	Fluid	Hydrogen	Scheme	Simple
Size function	Fixed	Solid	Aluminium	Gradient	Least Square Cells
Smoothing	Fine	Temperature	288 K	Discretisation pressure	Standard
Transition	Slow	Velocities	1, 3, 6, 9, 12 ms^{-1}	Momentum	Second order
Elements	250000 - 310000	Pressure Outlet	0	Porosity	0.90

385385

386   To obtain a comparison on the pressure drop in porous media, and to draw a contrast to the

387   simulation results obtained by ANSYS, the proposed mathematical models were analysed using

388   the values as shown in Table 3. Fig. 13 shows the pressure drop related to the different

389   mathematical models and the simulation result for design D4 from ANSYS. It is found that for the

390   same porosity $\zeta = 0.936$ and pore diameter, $d_p = 3.068$mm, the Darcy model, has the lowest

391   pressure drop which follows a similar trend to that of the pressure drop for design D4.

22

393 Table 3: Parameter values used in the mathematical models

Parameters	Values	Reference
ζ	0.936	[49]
v	1.838×10^{-5} (kg/s m)	[49]
ε	4	[48]
d_p	3.068 (mm)	[7]
τ	1.308	[49]
ρ	1.184 (kg/m$^{3)}$)	[49]
d_L	0.35 (mm)	[48]
α	0.4	[48]
L	5 (mm)	-

395   Using the established result, that the Darcy model fits well with the ANSYS model simulation for

396   design D4, further analysis on the mathematical model is therefore performed. The Darcy model

397   in equation (2) relates to the pressure drop as a function of the permeability and the fluid velocity.

398   The permeability as described in equation (3) relates to the pore diameter and the porosity.

399   Fig. 14 shows the effect of increasing pore diameter for a constant porosity, $\zeta = 0.93$. It is

400   observed that the permeability of the material exponentially increases while the C factor reduces

401   and approaches a constant value for higher pore diameter [39]. This suggests that the pressure drop

402   for high pore diameter would have a linear response with increasing flow velocity. This can be

403   observed in Fig. 15, where the effect of increasing pore diameter is shown with respect to the

404   increasing velocity and the pressure drop. Further analysis on the effect of increasing porosity

23

405   suggest that for higher porosity, the pressure drop is lower. This effect can be observed in Fig. 15

406   (b) for a pore diameter of 100 µm.

407407

408   Further utilisation of the Darcy model is carried out by analysing the overall effect on pressure

409   drop in a 3D surface plot where the effect of varying pore diameter, porosity, and the flow velocity

410   is considered. This can be observed in Fig. 16 (a), where a higher pore diameter and higher porosity

411   shows a low-pressure drop. There is, however, a trade-off with a low-pressure drop at higher pore

412412   diameter, which is the flow regime of the operating fuel cell. For a fully functional PEMFC, it has

413413   been established that the flow through the channel is laminar. The Reynolds Number $(R_e =$

414414 $\frac{\rho\sqrt{\gamma}V}{v})$ is a good measure of determining the flow in a channel, where, $R_e < 2300$ indicates a laminar

415415   flow and turbulent otherwise [59-60]. It is dependent on the flow velocity and the permeability

416   (pore diameter and porosity) of the channel, assuming a constant viscosity and density. This key

417   measure is analysed for varying porosity, pore diameter and flow velocity in Fig. 16 (b). It is

418   observed that for a flow velocity above 6 m/s and pore diameter of greater than 2 mm, the flow in

419   the channel would therefore be turbulent. This result indicate that in the design of OPCF channel

420   for consideration in PEM fuel cells, with higher pore diameter to achieve a low-pressure drop, the

421   flow velocity should be less than 6 m/s.

422   One clear way of analysing fuel cell performance is through the polarisation curve. It is expected

423   that, due to a low-pressure drop, fuel cell performance to be better. Mathematical models that

424   describe the polarisation curve has been extensively studied in the literature [38], however, the

425   performance can also be measured using a linear approximation of the polarisation curve, as this

426   works well for most fuel cells acting within their practical operating range [38]. In analysing such

427   performance, the permeability of the flow channel is a key parameter, which depends on the pore

24

428   diameter and the porosity for porous media. A linear approximation of the polarisation curve is

429   therefore developed which is dependent on the permeability of the channel as defined earlier in

430   equations (12) and (13). Fig. 17 shows a linear approximation of the polarisation curve for both

431   the porous medium and hollow (serpentine) channel. All of the terms in equation (13) are kept

432   constant for both types of channels except the permeability, which changes with the type of

433   channel, as defined in equations (3) and (4). Fig. 17 shows the effect of using porous channel on

434   the current density and cell potential. The result for the porous channel was evaluated for a pore

435   diameter of $d_p = 0.25$mm and porosity, $\zeta = 0.90$, whereas for the hollow serpentine channel, the

436   hydraulic diameter (calculated) $d_h = 0.5$ mm was taken. The calculated permeability of the

437   hollow channel was 2.02×10^{-8} m^2 and for the porous channel was 2.53×10^{-8} m^2. It is observed

438   in Fig. 17 that, due to a low-pressure drop because of the use of OPCF flow channel, the

439   performance of the PEM fuel cell is greatly increased. Based on the analysis carried out it can be

440   concluded that for a good performance of the PEM fuel cell using OPCF material, the permeability

441   should be greater than the traditional flow channel.

442442

443 TESTING OF FUEL CELL

444444

445   The fuel cell was also experimentally validated by testing the performance of the serpentine flow

446   plate design with that of an open pore cellular foam material used in the new design. Fig. 18 shows

447   the assembly process used in building the fuel cell with the open pore cellular foam material. The

448   grooves were cut using a CNC machine to create the position where the aluminium open pore

449   cellular foam will be placed. After the OPCFM is put in position, the membrane electrode assembly

450   obtained from fuel cell store was also carefully placed on the foam. The cathode housing was also

25

451 designed to have the foam as its flow channel. The fuel cell was carefully tightened and checked

452 for leaks, as any loss of hydrogen gas will compromise the economic efficiency of the new PEMFC

453 design. Once checks showed the fuel cell was well sealed, it was then placed in the experimental

454 set up as shown in Fig 19 and Fig.

455 The results obtained after using the open pore cellular foam material shown in Fig. 21 indicated

456 that the fuel cell performance improved appreciably compared to the serpentine design and this

457 also validated the results obtained computationally in ANSYS. It must be noted that the hydrogen

458 was passed through a humidification chamber to keep the membrane moist to aid in good electro

459 osmotic drag and back diffusion for both experiments. All other parameters, like cell operating

460 temperature and pressure, were kept constant for both experiments.   When the pressure drop

461 through the bipolar plate between the inlet and outlet is high, more pumping power will be needed

462 to overcome this, hence reducing the net performance of the fuel cell. The more gas is introduced

463 to the catalyst layer, the more electrons are released hence the reason for the high performance of

464 the fuel cell when the open pore cellular foam was used.

465 **CONCLUSION**

466 The general performance of a fuel cell depends highly on the pressure drop as well as the velocity

467 of the gas as it flows through the fluid domain. High drop in pressure indicates that the flow of gas

468 to the reactive site would be low. Therefore, the rate at which electrons will be released due to the

469 electrochemical reaction will be lower, leading to a lower current produced. The work also

470 identified that the design of the flow plate affects the water management of the fuel cell. Having a

471 design where there are dead zones implies that not all portions (surface) of the MEA will be utilised

472 during the electrochemical reaction. The orientations of the inlet and outlet also played a key role

473 in determining the efficiency of the fuel cell. The drop in pressure of the foam was only subject to

26

474 the pores of the foam while that of the serpentine design experienced pressure drop in each arm of

475 the flow channel. It explains the high-pressure drop for the serpentine flow plate design. The work

476 finally concluded that, in comparison to the serpentine flow design, the open pore cellular foam

477 material was a suitable option for a fuel cell with a minimum pressure drop of 22.5 Pa as compared

478 to 10,000 Pa with the serpentine design at a velocity of 12 m/s.

479 REFERENCES

480 1. Tabbi Wilberforce, A. Alaswad, A. Palumbo, A. G. Olabi. Advances in stationary and

481   portable fuel cell applications. International Journal of Hydrogen Energy 41(37) March

482   2016.

483 2. Tabbi Wilberforce, Ahmed Al Makky, A. Baroutaji, Rubal Sambi, A.G. Olabi.

484   Computational Fluid Dynamic Simulation and modelling (CFX) of Flow Plate in PEM fuel

485   cell using Aluminum Open Pore Cellular Foam Material. Power and Energy Conference

486   (TPEC), IEEE, Texas. 2017. DOI: 10.1109/TPEC.2017.7868285

487

488 3. Tabbi Wilberforce, Ahmed Al Makky, A. Baroutaji, Rubal Sambi, A.G. Olabi

489   Optimisation of bipolar plate through computational fluid dynamics simulation and

490   modelling using nickle open pore cellular foam material. International conference on

491   reneable energies and power quality (ICREPQ'17), ISSN 2171-038X, No 15 April 2017

492

493 4. Tabbi Wilberforce, A. Alaswad, J. Mooney,A.G.Olabi.Hydrogen Production for Solar

494   Energy Storage. A Proposed Design Investigation.Proceedings of the 8th International

495   Conference on sustainable Energy and Environmental Protection. ISBN: 978-1-903978-

496   52-8

27

497   5. Baroutaji, A., Carton, J, G., Stoke, J., Olabi, A, G., 2014. Design and Development of

498   Proton Exchange Membrane Fuel cell using the Open Pore Cellular Foam as flow plate

499   material. Journal of Energy Challenges and Mechanics. Volume 1 (2014) issue 3.

500   6. Mikkola, M., 2001. Experimental studied on Polymer Electrolyte Membrane fuel cells

501   stacks. Helsinki University of Technology, Department of Engineering Physics and

502   Mathematics, Masters Thesis.

503   7. Carton, J. G., Olabi, A. G. Representative model and flow characteristics of open pore

504   cellular foam and potential use in proton exchange membrane fuel cells. International

505   Journal Of Hydrogen Energy 40 (2015) 5726 – 5738.

506   8. T. Wilberforce, Z. El-Hassan, F.N. Khatib, A. Al Makyy, A. Baroutaji, J. G. Carton and A.

507   G. Olabi, Modelling and Simulation of Proton Exchange Membrane Fuel cell with

508   Serpentine bipolar plate using MATLAB, International journal of hydrogen, 2017. DOI:

509   10.1016/j.ijhydene.2017.06.091.

510   9. J. G. Carton, V. Lawlor, A. G. Olabi, C. Hochenauer and G. Zauner, "Water droplet

511   accumulation and motion in PEM fuel cell mini-channels", Energy, 39 (1), pp 63-73, 2012

512   10. Olabi AG. The 3rd international conference on sustainable energy and environmental

513   protection SEEP 2009 the guest editor's introduction. Energy 2010;35:4508-9

514   11. V. Lawlor, S.Griesser, G.Buchinger, A.G.Olabi, S. Cordiner and D. Meissner, "Review

515   of the micro-tubular solid oxide fuel cell: Part I. Stack design issues and research

516   activities", J.Power Sources,193 (2),pp 387-399, 2009.

517   12. S. K. Dong, B. T. Yun and D. K. Lee, "Design and numerical study for l kW tubular SOFC

518   APU system", Anonymous Fuel Cell Seminar, San Antonio; TX; United states:

519   Electrochemical Society, Inc, October, pp- 701-706, 2007.

520   13. Tabbi Wilberforce, Zaki, El-Hassan, F.N. Khatib, A. Al Makyy, A. Baroutaji, J. G.

521   Carton and A. G. Olabi. Developments of electric cars and fuel cell hydrogen electric

522   cars. DOI: 10.1016/j.ijhydene.2017.07.054

523   14. Cook B. Introduction to fuel cells and hydrogen technology. Eng. Sci. Educ. J. 2002; 11(6):

524   205 – 16.

525   15. Superamaniam S. Fuel Cells: from fundamentals to applications. New York: Springer

526   Science & Business Media: 2006.

527   16. Tsuchiya H, Kobayashi, O. Mass production of PEM fuel cell by learning curve.

528   International Journal on Hydrogen Energy 2004; 29:985 – 90.

529   17. Chang HP, Chou CL, Chen Ys, Hou Ti, Weng BJ. The design and cost analysis of a

530   portable PEMFC UPS system. International Journal on Hydrogen Energy 2007; 32:316 –

531   22.

532   18. Afsari E, Jazayeri SA. Effects of the cell thermal behavior and water phase change on a

533   proton exchange membrane fuel cell performance. Energy Convers Manage 2010; 51: 655

534   – 62

535   19. A. D. Le and B. Zhou "A generalized numerical model for liquid water in a proton

536   exchange membrane fuel cell with interdigitated design", J.Power Sources ,193 (2), pp

537   665683,2009.

538   20. A. Kazim, H. T. Liu and P. Forges, "Modelling of performance of PEM fuel cells with

539   conventional and interdigitated flow fields", J.Appl.Electrochem, 29 (12), pp 1409-

540   1416,1999.

541   21. J.P Kloess, X. Wang, J. Liu, Z. Shi and L. Guessous, "Investigation of bio-inspired flow

542   channel designs for bipolar plates in proton exchange membrane fuel cells", J.Power

543   Sources, 188(1), pp 132-140, 2009.

544   22. Yoon YG, Lee WY, Park GG, Yang TH, Kim CS. Effects of channel and rib widths of

545   flow field plates on the performance of a PEMFC. International Journal Hydrogen Energy

546   2005; 30:1363 – 6

547   23. Wang XD, Yan WM, Duan YY, Weng FB, Jung GB, Lee CY. Numerical study on channel

548   size effect for proton exchange membrane fuel cell with serpentine flow field. Energy

549   convers Manage 2010; 51:959 – 68.

550   24. Su A, Weng FB, Hsu CY, Cheng YM. Studies on flooding in PEM fuel cell cathode

551   channels. International Journal Hydrogen Energy 2006; 31:1031 – 9.

552   25. Venkatraman M, Shimpalee S, Van Zee JW, Moon SI, Extrand CW. Estimates of pressure

553   gradients in PEMFC gas channels due to blockage by static liquid drops, International

554   Journal Hydrogen Energy 2009;34:5522 – 8.

555   26. Zhang HF, Pei PC, Yuan X. The conception of in – plate adverse – flow field for a proton

556   exchange membrane fuel cell. International Journal Hydrogen Energy 2010; 35:9124 – 33.

557   27. Yazdi MZ, Kalbasi M. A novel analytical analysis of PEM fuel cell. Energy convers

558   Manage 2010; 51:241 – 6.

559   28. Yan WM, Liu HC, Soong CY, Chen F, Cheng CH. Numerical study on cell performance

560   and local transport phenomena of PEM fuel cells with novel flow field designs. Journal

561   Power Sources 2006; 161:907 – 19.

30

562 29. Wang XD, Duan YY, Yan WM, Lee DJ, Su A, Chi PH. Channel aspect ratio effect for

563   proton exchange membrane fuel cell with serpentine flow field: role of sub – rib

564   convection. Journal Power Sources 2009; 193: 684 – 90.

565 30. A.P. Manso, F. F. Marzo, J. Barranco, X. Garikano, and M. Garmendia. Mujika, "Influence

566   of geometric parameters of the flow fields on the performance of a PEM fuel cell. A

567   review", International Journal of Hydrogen Energy, 37 (20), pp 15256-15287, 2012.

568 31. Tseng, Chung-Jen, *et al.* "A PEM fuel cell with metal foam as flow distributor."Energy

569   Conversion and Management 62 (2012): 14-21.

570 32. C.J. Tsang, B.T. Tsai, Z.S. Liu, T.C. Cheng, W.C. Chang and S.K. Lo,"Effects of flow

571   field design on the performance of a PEM fuel cell with metal foam as the flow distributor",

572   International Journal of Hydrogen Energy, 37 (17), pp 13060-13066, 2012.

573 33. A. Kumar and R.G. Reddy, "Materials and design development for bipolar/end plates in

574   fuel cells", J Power Sources, 129 (1), pp 62-67, 2004.

575 34. A. Kumar, R.G. Reddy, "Modeling of polymer electrolyte membrane fuel cell with metal

576   foam in the flow-field of the bipolar/end plates", J Power Sources, 114 (1),pp 54-62, 2003.

577 35. Maricle DL, Nagle DC. Carbon foam fuel cell components. US Patent 4,125,676; 1978.

578   http://www.virginia.edu/ms/research/wadley/Documents/Publications/Titanium_Matrix_

579   Composite_Lattice_Structure.pdf [Accessed: 16/10/2016]

580 36. C.J. Tsang, B.T. Tsai, Z.S. Liu, T.C. Cheng, W.C. Chang and S.K. Lo,"Effects of flow

581   field design on the performance of a PEM fuel cell with metal foam as the flow distributor",

582   International Journal of Hydrogen Energy, 37 (17), pp 13060-13066, 2012

583 37. Kumar A, Reddy RG. Materials and design development for bipolar/end plates in fuel cells.

584   J Power Sources 2004; 129:62 – 7.

31

38. B. Ramos-Alvarado, A. Hernandez-Guerrero, F. Elizalde-Blancas and M.W. Ellis,"Constructal flow distributor as a bipolar plate for proton exchange membrane fuel cells", International Journal of Hydrogen Energy, 36 (20), pp 1296512976, 2011.

39. Wang, Y. Porous-Media Flow Fields for Polymer Electrolyte Fuel cells. Journal of the Electrochemical Society. 156(10) B1124 – b1133(2009)

40. Mathias, M, Roth, J, Fleming and Lernert W. Handbook of fuel cells: Fundamentals, Technologies and Applications. Vielstich W., Gasteiger H, Lamm Editors, Vol 3, John Wiley & Sons, New York (2003).

41. Medraj M, Baril, E, Loya V. The effect of microstructure on the permeability of metallic foam. J Mater Sci (2007) 42:4372-4383

42. Lage JL(1998) In: Ingham BD, Pop I (eds) Transport phenomena in porous media. Pp 1-30.

43. Gerbaux O, Buyens F, Mourzenko VV, Memponteil A, Vabre A, Thovert J-, *et al.* Transport properties of real metallic foams. J Colloid Interface Sci 2010 2/1;342(1):155-65

44. Zahi I, Rossi C, Faucheux V. Micro PEM fuel cell current collector design and optimization with CFD 3D modeling. Int J Hydrogen Energy 2011 11;36(22):14562-72.

45. Kim TH, Lee W, Jeong JH. Thermo-fluidic characteristics of open cell metal foam as an anodes for DCFC, part I: head loss open cell metal foam as an anodes for DCFC, part I: head loss 2014;39(23):12369-76

32

46. Wilson L, Narasimhan A, Venkateshan SP. Permeability and form coefficient measurement of porous inserts with non darcy model using non-plug flow experiments. J Fluids Eng Trans ASME 2006;128(3):638-42

47. Dukhan N. Correlations for the pressure drop for flow through metal foam. Exp Fluids 2006 10;41(4):665-72.

48. Ashby MF, Evans AG, Fleck NA, Gibson LJ, Hutchinson JW, Wadley HNG. Metal foams: a design guide. 1st ed. Massachusetts: Butterworth-Heinemann; 2000.

49. Du Plessis P, Montillet A, Comiti J, Legrand J. Pressure drop prediction for flow through high porosity metallic foams. Chem Eng Sci 1994;49(21):3545-53.

50. Kumar A, Reddy RG. Modelling of Polymer electrolyte membrane fuel cell with metal foam in the flow field of the bipolar/ end plates. J Power Sources 2003; 114: 54 – 62.

51. H. Liu and P. Li, "Even distribution/dividing of singlephase fluids by symmetric bifurcation of flow channels" International Journal of Heat and Fluid Flow, 40, pp 165-179, 2013.

52. H. Liu, P. Li and J.V. Lew,"CFD study on flow distribution uniformity in fuel distributors having multiple structural bifurcations of flow channels", International Journal of Hydrogen Energy, 35 (17), pp 9186-9198, 2010

53. G.M. Imbrioscia and H.J. Fasoli, "Simulation and study of proposed modifications over straight-parallel flow field design", International Journal of Hydrogen Energy, 39 (16), pp 8861-8867 (2014).

33

627   54. A. Kumar and G.R. Reddy, "Effect of channel dimensions and shape in the flow-field

628   distributor on the performance of polymer electrolyte membrane fuel cells", Journal of

629   Power Sources, 113 (1), pp 11-18, 2003.

630   55. E. Hontanon, M. J. Escudero, C. Bautista, P. L. GarcıaYbarra, and L. Daza, "Optimisation

631   of flow-field in polymer electrolyte membrane fuel cells using computational fluid

632   dynamics techniques." Journal of Power Sources, 86(1), pp 363368, 2000.

633   56. M. Mohammadi, G.N. Jovanovic and K.V. Sharp "Numerical study of flow uniformity and

634   pressure characteristics within a microchannel array with triangular manifolds" Computers

635   & Chemical Engineering, 52, pp 134144, 2013

636   57. A. Lozano, L. Valiño, F. Barreras, R. Mustata, "Fluid dynamics performance of different

637   bipolar plates: Part II. Flow through the diffusion layer", Journal of Power Sources, 179

638   (2), pp 711–722, 2008.

639   58. F. Barreras, A. Lozano, L. Valiño, C. Marín, A. Pascau, "Flow distribution in a bipolar

640   plate of a proton exchange membrane fuel cell: experiments and numerical simulation

641   studies", Journal of Power Sources, 144 (1), pp 54–66, 2005.

642   59. Colleen, S. S., Designing & Building of fuel cell, 1st ed. ISBN 0-07-148977-0, McGraw –

643   Hil, 2007.

644   60. Colleen, S. S., PEM Fuel Cell, Modelling, Simulation Using MATLAB. ISBN 978-0-12-

645   374259-9, Academic Press, 2008.

646
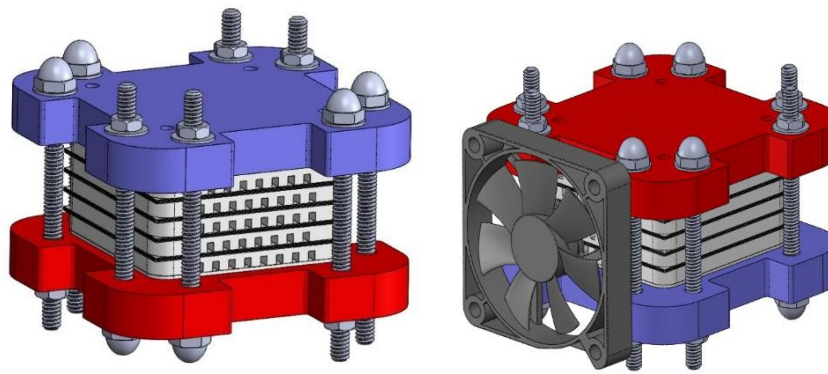
Fig. 1: Fuel cell with five (5) Stacks
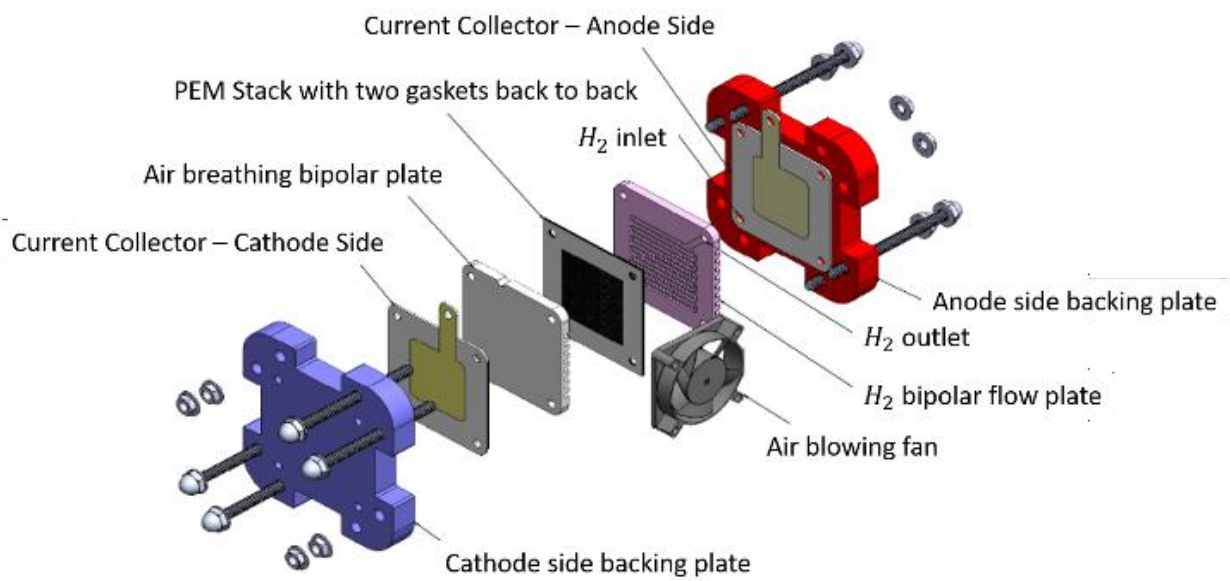
Fig. 2: Exploded view of a Proton Exchange Membrane fuel cell.
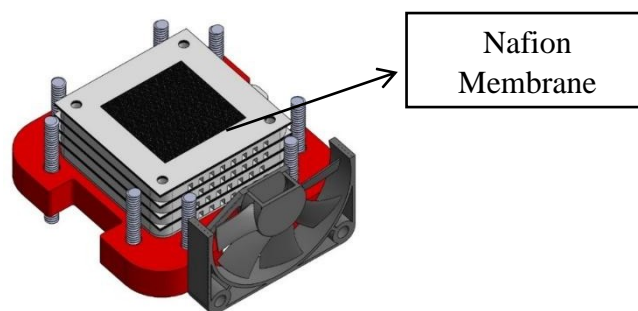
Fig. 3: Nafion Membrane Electrode assembly
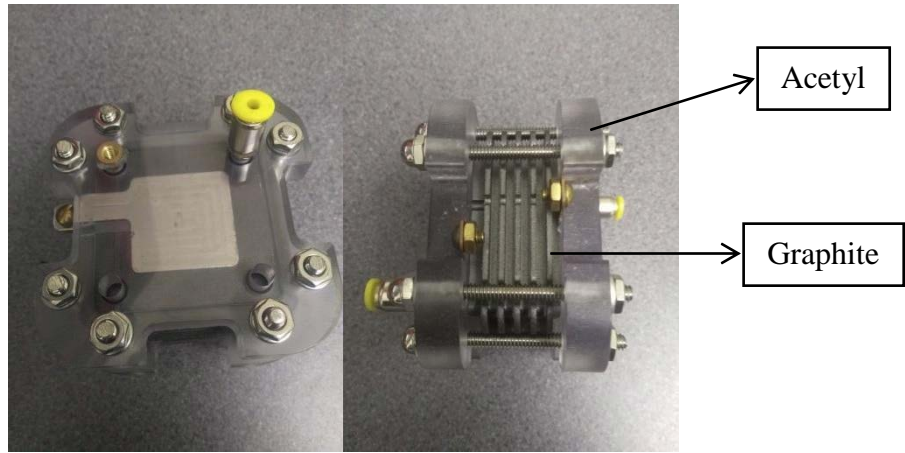
Fig. 4: PEM fuel cell with acetyl housing unit from obtained from fuel cell store.
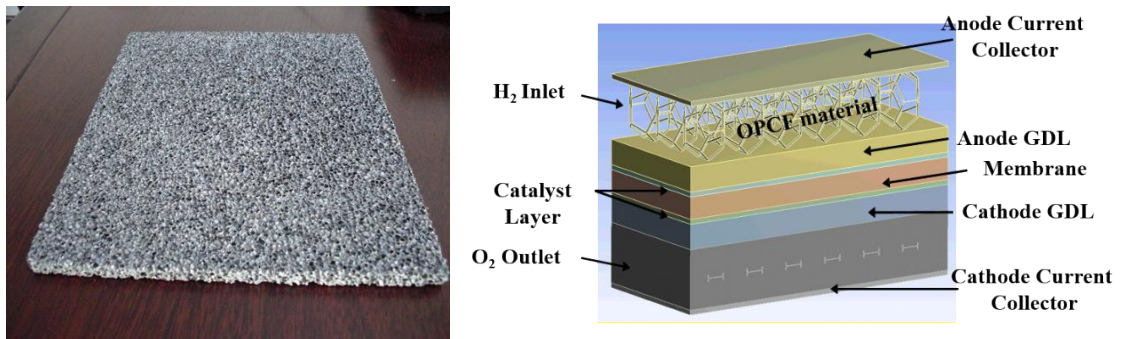
Fig. 5: OPCF material and the PEM Fuel cell schematic
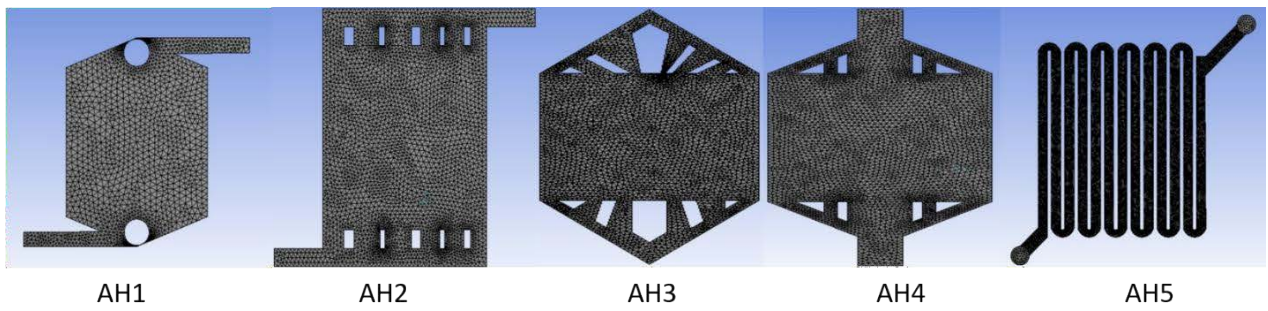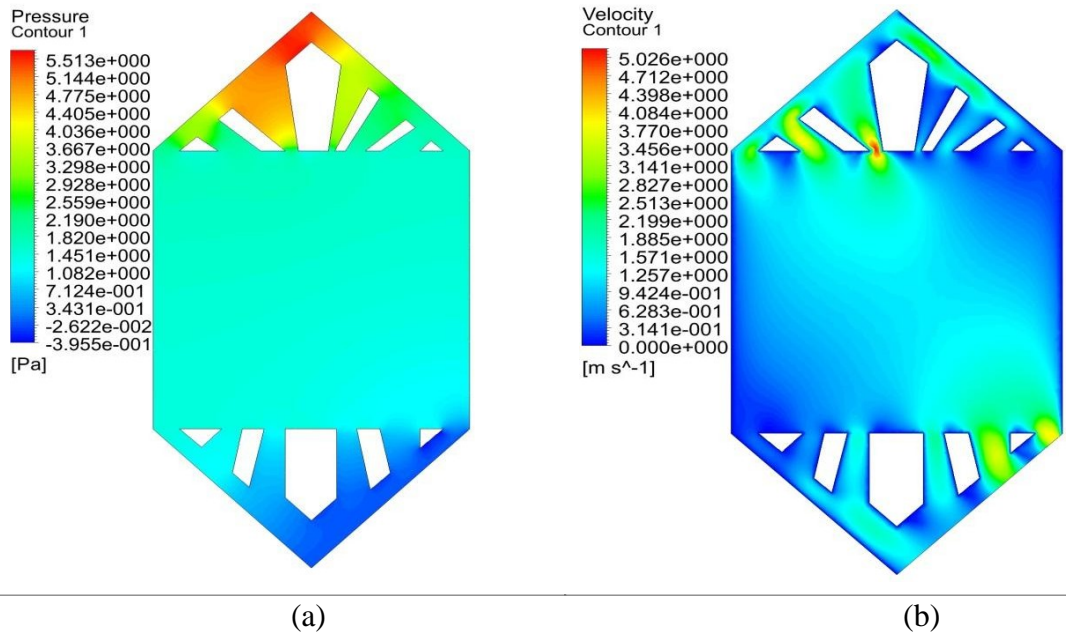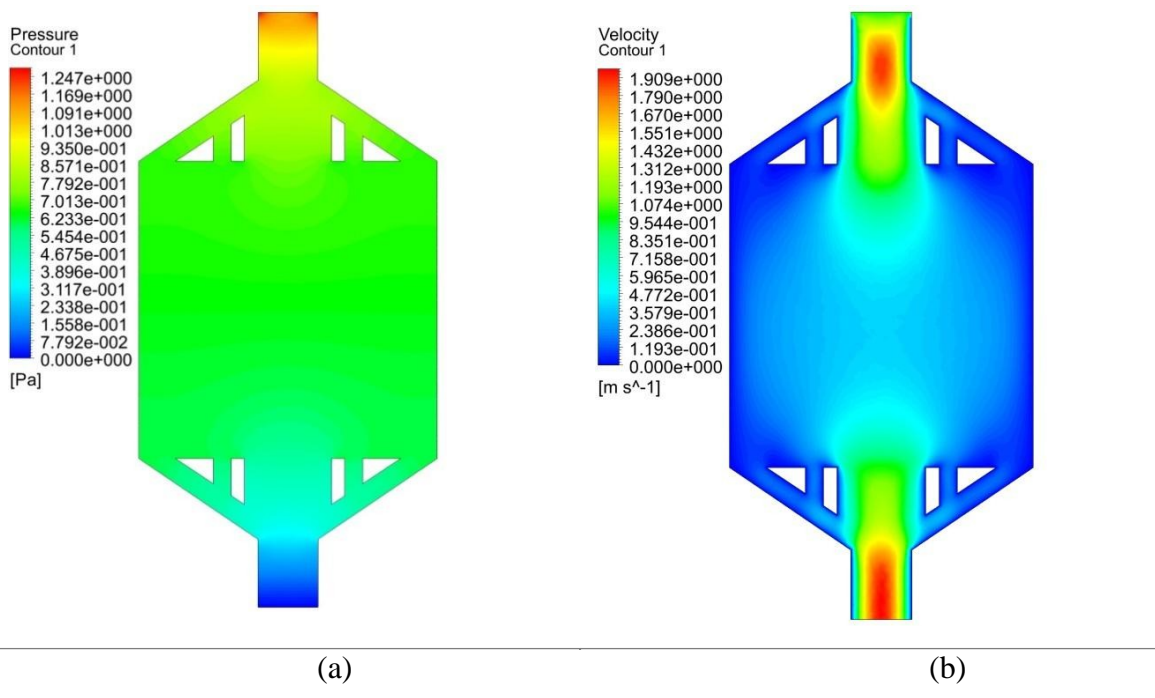

Fig. 6: The CFD model mesh using CFX.
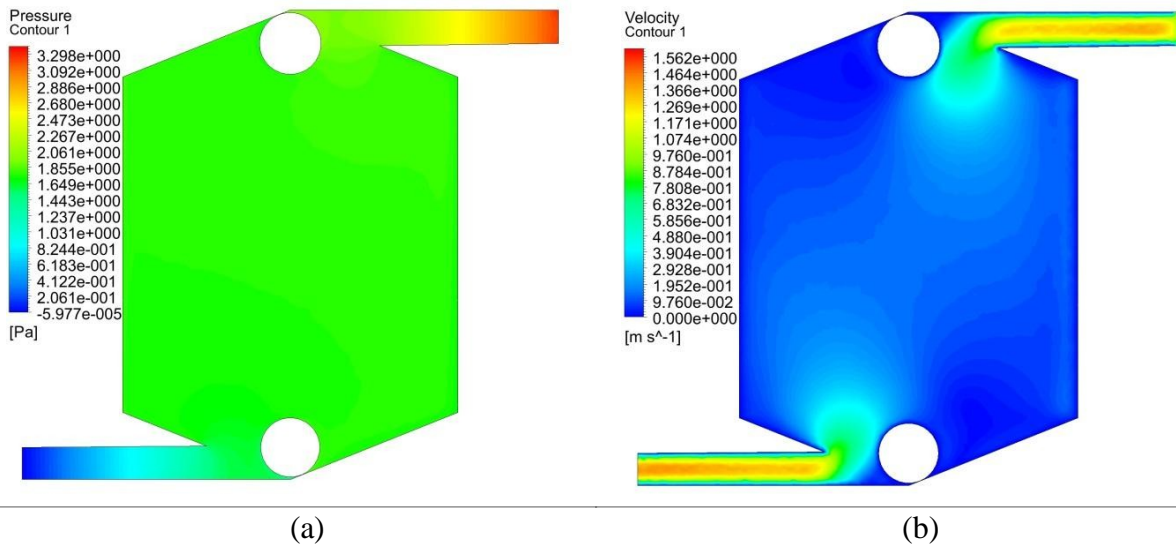
Fig. 7: Fluid domain for flow channel D1: (a) - pressure profile (Pa), (b) - velocity
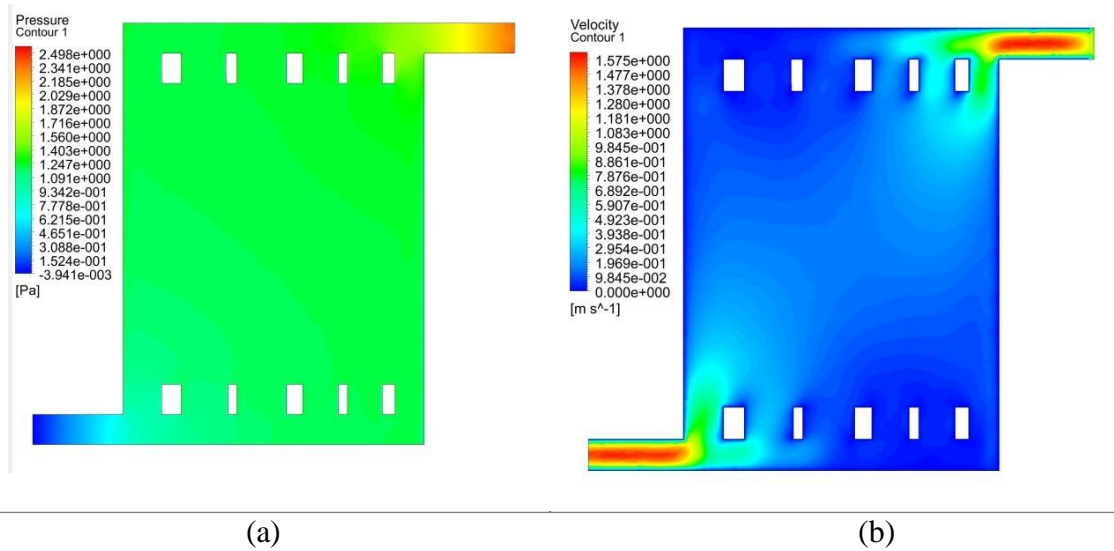
profile(m/s)

Fig. 8: Fluid domain for flow channel D2: (a) - pressure profile (Pa), (b) - velocity
profile(m/s)

Fig. 9: Fluid domain for flow channel D3: (a) - pressure profile (Pa), (b) - velocity profile(m/s)

Fig. 10: Fluid domain for flow channel D4: (a) - pressure profile (Pa), (b) - velocity profile(m/s)
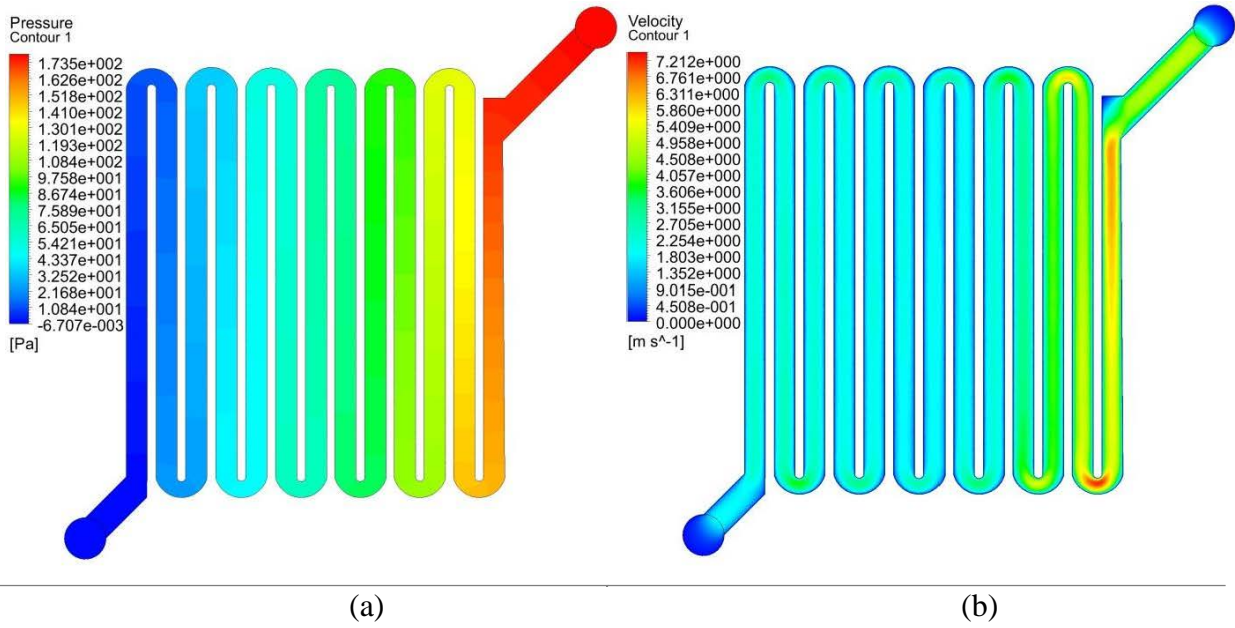
Fig. 11: Fluid domain for flow channel D5: (a) - pressure profile (Pa), (b) - velocity profile(m/s)
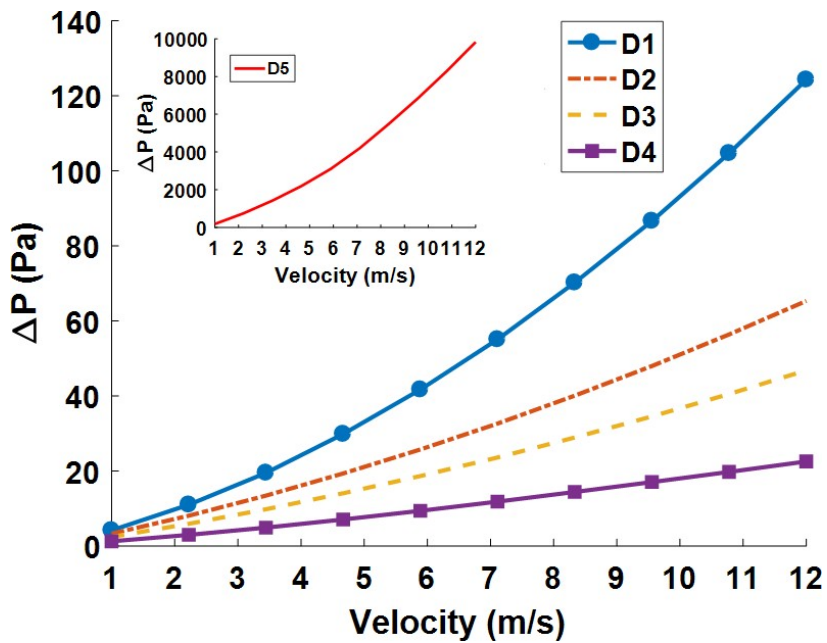
Fig. 12: Graph of velocity against pressure drop for flow channel designs D1 to D5.
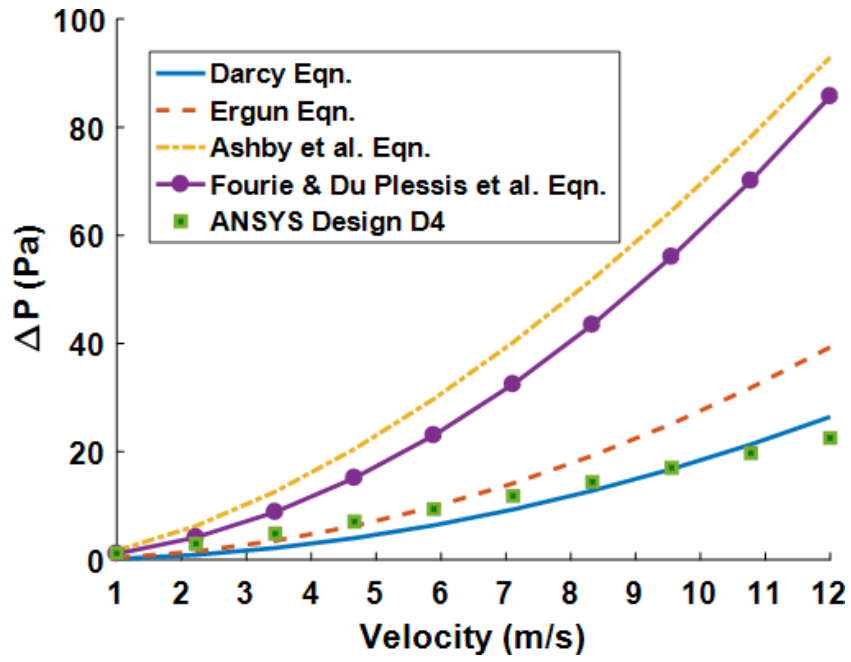
Fig. 13: Comparison of pressure drop using the different mathematical models and ANSYS simulation result for design D4.
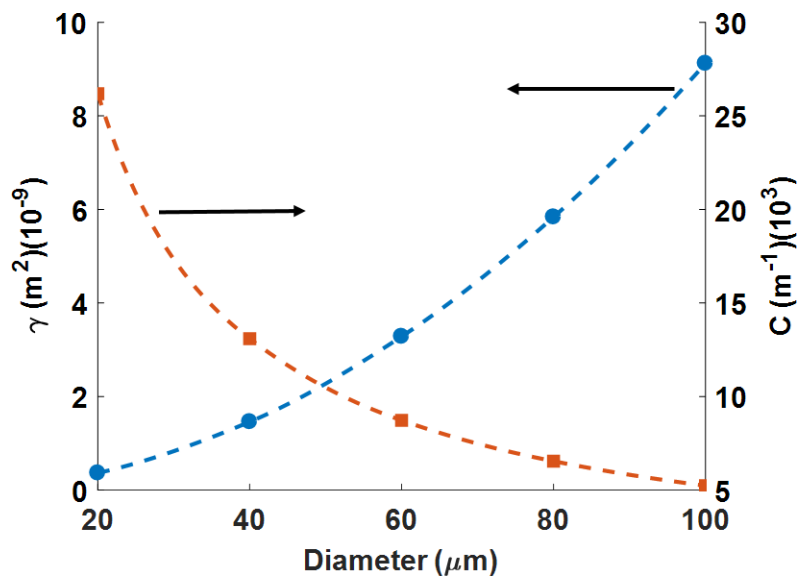
Fig. 14: Effect of increasing pore diameter on the permeability and factor C.
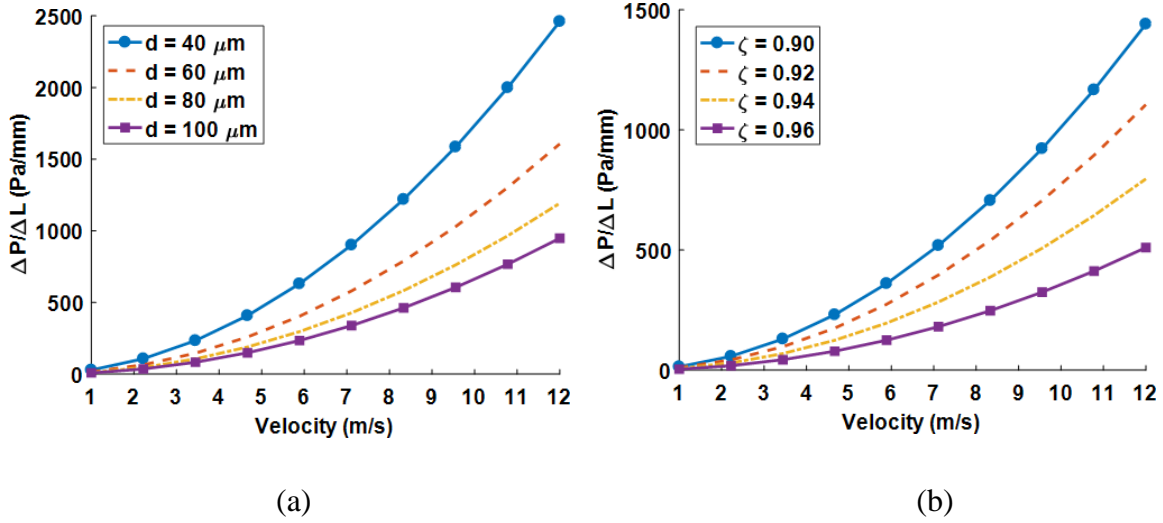
Fig. 15: Effect of increasing velocity on pressure drop for (a) different pore diameter (b) different material porosity.
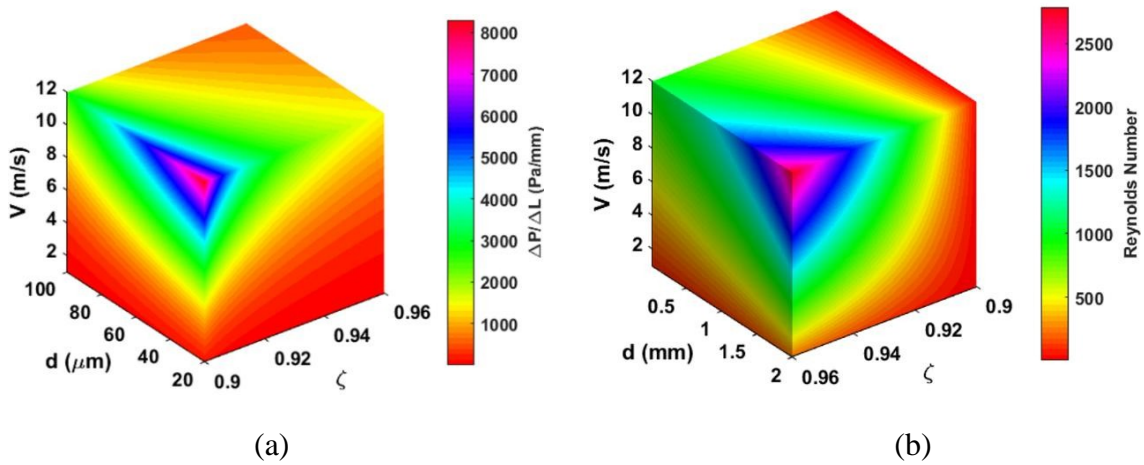
Fig. 16: Surface plot at varying pore diameter, porosity and flow velocity for (a) Pressure drop (b) Reynolds Number
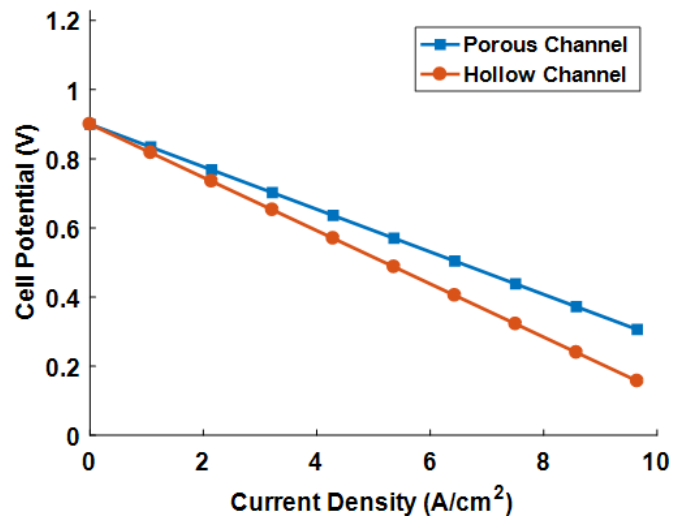
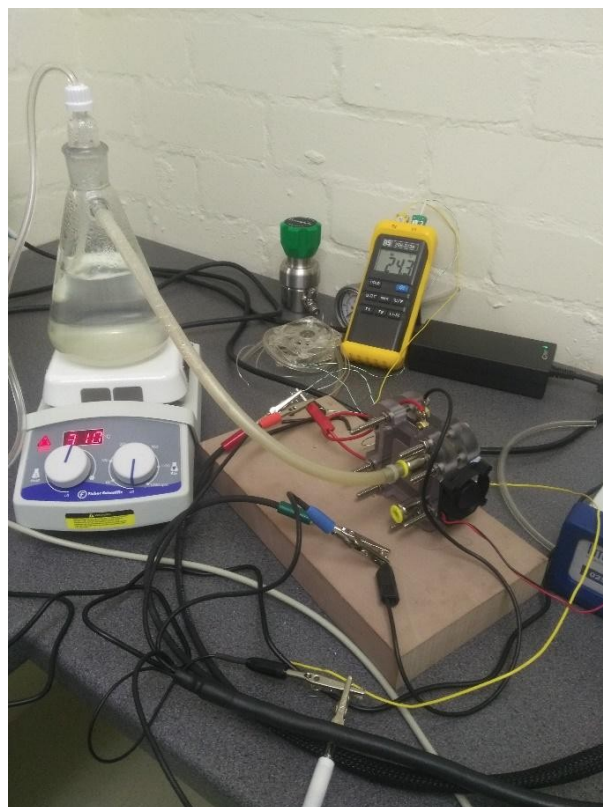Fig. 17: Current density vs cell potential for the porous and hollow channel.
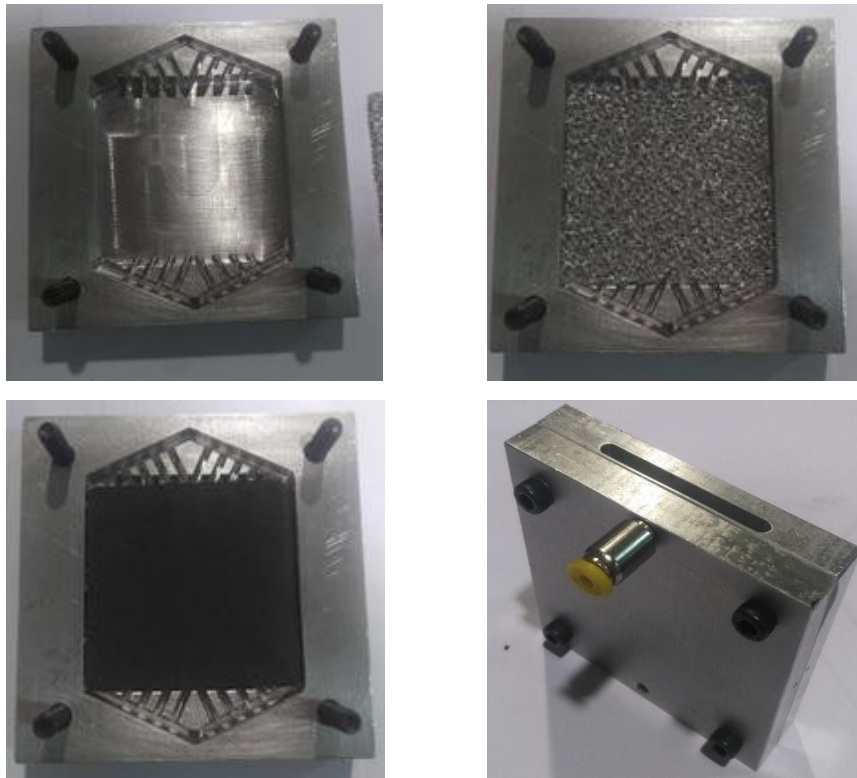
Fig. 18 Building of Open pore cellular foam material PEMFC.
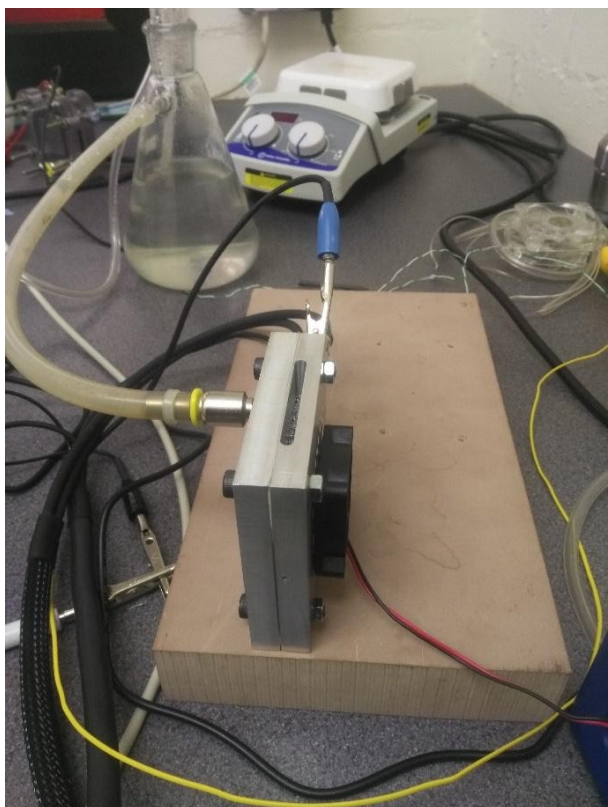
a)

b)

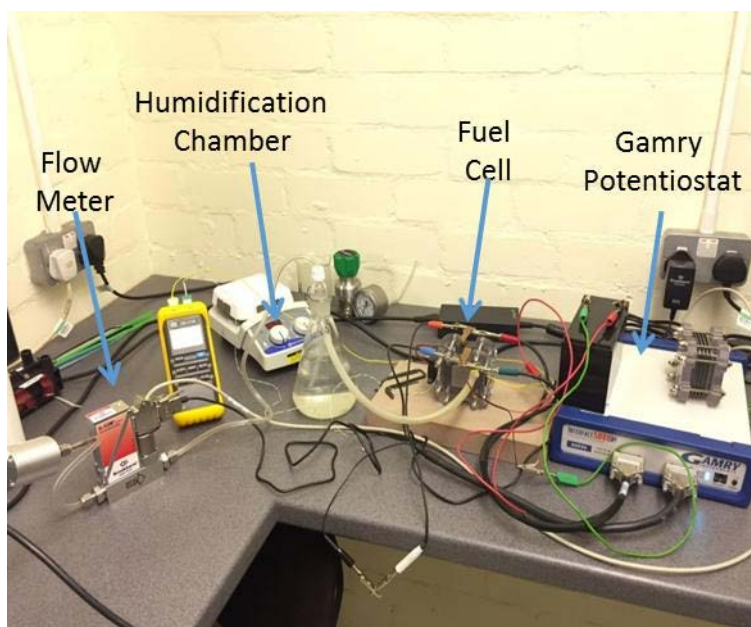Fig. 19: Experimental set up a) Open pore cellular foam material   b) Serpentine flow field design

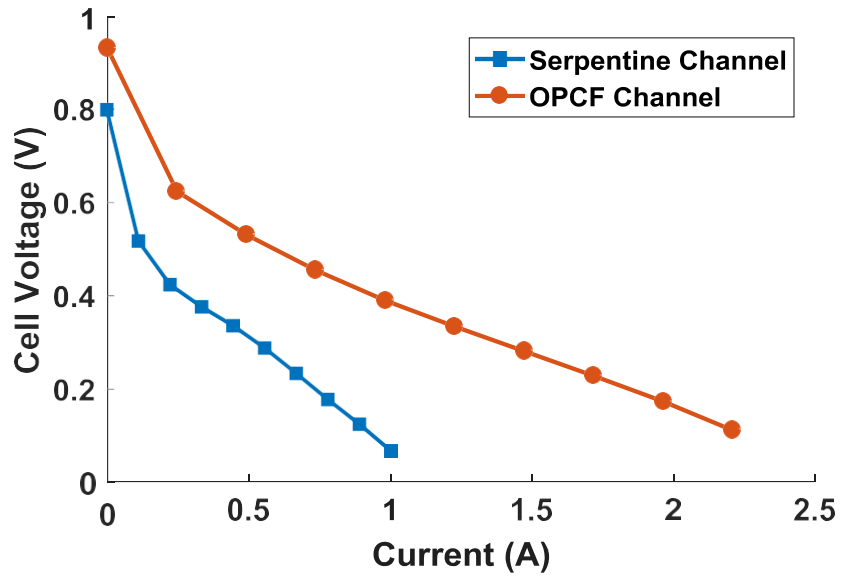Fig 20: Experimental set up for the texting of the fuel cell

Fig. 21: Polarisation curve for the serpentine flow field and the open pore cellular foam material